Supporting Information to

A 3D Time-Shared NOESY Experiment Designed to Provide Optimal Resolution for Accurate Assignment of NMR Distance Restraints in Large Proteins.

Subrata H. Mishra, Bradley J. Harden, Dominique P. Frueh*.

Department of Biophysics and Biophysical Chemistry, Johns Hopkins University, School of Medicine, Baltimore, MD, 21205 U.S.A

TS – HN-TROSY / HC-HSQC-NOESY.

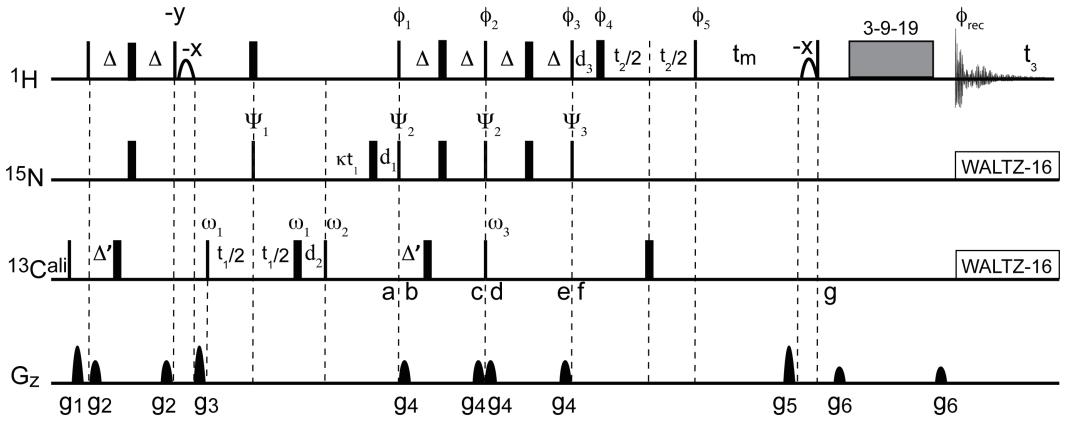

Figure 1. Pulse sequence of the 3D TS – HN-TROSY / HC-HSQC-NOESY experiment. Narrow and wide bars represent 90° and 180° hard pulses, respectively. All pulses are applied along the x axis unless mentioned otherwise. The empty ellipsoids represent water-selective 90° rectangular pulses. The block labeled 3-9-19 is a WATERGATE water suppression scheme[1]. The delays are $\Delta=1/(4J_{NH})$, $\Delta'=1/(4J_{CH})$ and, t_m = 150 ms (mixing time). The delays d1 = 3* pw_C + pw_N, d2 = pw_N, and d3 = 2*pw_C are used to prevent first order phase corrections in indirect dimensions; pw_C and pw_N are the 90° pulse widths for ^{13}C and ^{15}N nuclei, respectively. The time-shared evolution of ^{15}N and ^{13}C coherences has been implemented as published previously.[2] κ = SW(C)/SW(N) – ½ with SW(C) and SW(N) the spectral widths of ^{13}C (24 ppm) and ^{15}N (35 ppm), respectively. The filled ellipsoids (line labeled G_z) are 1 ms smoothed-square shaped-pulse gradients: g_1= -36 G/cm, g_2 = 7.5 G/cm, g_3 = 25.5 G/cm, g_4 = 2.5 G/cm, g_5 = -40 G/cm and g_6 = 4 G/cm; each gradient pulse is followed by a 200 μs recovery delay. ^{13}C and ^{15}N decoupling during detection are both achieved using WALTZ-16 sequences[3], with field strengths of 0.71 kHz. Simultaneous ^{13}C and ^{15}N decoupling necessitates the use of lower field strengths and synchronous pulsing to prevent artifacts[4]. The pulse phases detailed henceforth are spin-dynamic phases and should be modified appropriately depending on the NMR spectrometer used[5]. Spin state selection (^{15}N) and quadrature detection in both indirect dimensions (t_1 & t_2) is achieved by post-acquisition combinations of transients that are recorded and stored separately (S6: Table 4, S7:Table 5). These transients have the following phase settings:

A1: ϕ_1 =y, ϕ_2 =x, ϕ_3 = -x, ψ_1 = y -y, ψ_2 =-y, ψ_3 = x, ω_1 =x -x, ω_2 =x, ω_3 = x x -x -x ;

A2: ϕ_1 =x, ϕ_2 =y, ϕ_3 = -y, ψ_1 = y -y, ψ_2 =-x, ψ_3 = y, ω_1 =y -y, ω_2 =x, ω_3 = x x -x -x ;

A3: ϕ_1 =y, ϕ_2 =x, ϕ_3 = x, ψ_1 = y -y, ψ_2 =-y, ψ_3 = x, ω_1 =x -x, ω_2 =x, ω_3 = x x -x -x ;

A4: ϕ_1 =x, ϕ_2 =y, ϕ_3 = y, ψ_1 = y -y, ψ_2 =-x, ψ_3 = y, ω_1 =y -y, ω_2 =x, ω_3 = x x -x -x ;

It should be noted that the 4-step phase cycle in each transient is used to remove artifacts and not for quadrature detection and line-selection mentioned in S6. A1 to A4 are recorded either with ϕ_4= -y and ϕ_5= x ($A1_x$ to $A4_x$) or with ϕ_4= x and ϕ_5=y ($A1_y$ to $A4_y$), where the subscript denotes the phase of ϕ_5. The next section discusses how these 8 transients are combined to provide frequency discrimination in all dimensions simultaneously with selection of the HN-TROSY (Table 3). ϕ_{rec} = x -x x –x, for all transients. To delineate ^{15}N and ^{13}C edited spectra, these 8 transients are recorded a second

time with the phase of ω_2 inverted. During processing the transients in which ω_2 has opposite phases add to yield the ^{15}N pathway and subtract to yield the ^{13}C pathway. TPPI[6] is implemented during t_1 evolution using the phases ψ_1, ω_1 and ϕ_{rec}. The 90° ^{13}C pulse applied at point d is used to cancel weak dispersive artifacts which result from incomplete conversion of strong methyl proton antiphase coherences into in-phase coherences in the period b to c. All experiments were conducted at 25 °C on a 600 MHz Bruker Avance III spectrometer equipped with a CP-QCI $^{1}H/^{31}P/^{13}C/^{15}N$-$^{2}H$ cryoprobe™ with a single axis gradient coil. Both Bruker and Agilent pulse programs can be obtained by contacting the authors.

Product operator analysis of the 3D TS – HN-TROSY / HC-HSQC-NOESY experiment.

The beginning of the pulse sequence uses a time-shared INEPT element[7, 8] to convert amide and methyl proton polarizations into ^{15}N and ^{13}C single-quantum coherences (SQCs), respectively. Using a scheme designed by Permi and co-workers[2], ^{15}N SQCs evolve during t_1 and benefits from attenuated transverse relaxation, while evolution under J_{CH} is refocused for methyl moieties during t_1. Table 1 shows the density operator elements involving amide groups, starting from point a and ending at point f. Table 2 shows the density operator elements involving methyl groups, starting from point b and ending at point f. Finally, Table 3 shows the density operator elements at point g and, thus, encompasses evolution during t_2.

	a	b	c	d	e	f	
A_1	$-2\,{}^{N}H_zN_x$	$2\,{}^{N}H_xN_z$	${}^{N}H_y$	${}^{N}H_z$	$-\,{}^{N}H_z$	$-\,{}^{N}H_y$	$½\,(c^+_N + c^-_N)$
	$-N_y$	$-N_y$	$2\,{}^{N}H_zN_x$	$2\,{}^{N}H_yN_z$	${}^{N}H_x$	${}^{N}H_x$	$½\,(s^+_N - s^-_N)$
	$-2\,{}^{N}H_zN_y$	$-2\,{}^{N}H_xN_y$	$2\,{}^{N}H_xN_y$	$2\,{}^{N}H_xN_y$	$-2\,{}^{N}H_xN_y$	$2\,{}^{N}H_xN_z$	$½\,(s^+_N + s^-_N)$
	N_x	$-N_z$	N_z	N_x	$-2\,{}^{N}H_zN_y$	$2\,{}^{N}H_yN_z$	$½\,(c^-_N - c^+_N)$
A_2	$-2\,{}^{N}H_zN_x$	$2\,{}^{N}H_yN_x$	$-2\,{}^{N}H_yN_x$	$-2\,{}^{N}H_yN_x$	$2\,{}^{N}H_yN_x$	$2\,{}^{N}H_yN_z$	$½\,(c^+_N + c^-_N)$
	$-N_y$	$-N_z$	N_z	$-N_y$	$2\,{}^{N}H_zN_x$	$-2\,{}^{N}H_xN_z$	$½\,(s^+_N - s^-_N)$
	$-2\,{}^{N}H_zN_y$	$2\,{}^{N}H_yN_z$	${}^{N}H_x$	$-\,{}^{N}H_z$	${}^{N}H_z$	$-\,{}^{N}H_x$	$½\,(s^+_N + s^-_N)$
	N_x	N_x	$-2\,{}^{N}H_zN_y$	$-2\,{}^{N}H_xN_z$	$-\,{}^{N}H_y$	$-\,{}^{N}H_y$	$½\,(c^-_N - c^+_N)$
A_3	$-2\,{}^{N}H_zN_x$	$2\,{}^{N}H_xN_z$	${}^{N}H_y$	${}^{N}H_z$	$-{}^{N}H_z$	${}^{N}H_y$	$½\,(c^+_N + c^-_N)$
	$-N_y$	$-N_y$	$2\,{}^{N}H_zN_x$	$2\,{}^{N}H_yN_z$	${}^{N}H_x$	${}^{N}H_x$	$½\,(s^+_N - s^-_N)$
	$-2\,{}^{N}H_zN_y$	$-2\,{}^{N}H_xN_y$	$2\,{}^{N}H_xN_y$	$2\,{}^{N}H_xN_y$	$-2\,{}^{N}H_xN_y$	$2\,{}^{N}H_xN_z$	$½\,(s^+_N + s^-_N)$
	N_x	$-N_z$	N_z	N_x	$-2\,{}^{N}H_zN_y$	$-2\,{}^{N}H_yN_z$	$½\,(c^-_N - c^+_N)$
A_4	$-2\,{}^{N}H_zN_x$	$2\,{}^{N}H_yN_x$	$-2\,{}^{N}H_yN_x$	$-2\,{}^{N}H_yN_x$	$2\,{}^{N}H_yN_x$	$2\,{}^{N}H_yN_z$	$½\,(c^+_N + c^-_N)$
	$-N_y$	$-N_z$	N_z	$-N_y$	$2\,{}^{N}H_zN_x$	$2\,{}^{N}H_xN_z$	$½\,(s^+_N - s^-_N)$
	$-2\,{}^{N}H_zN_y$	$2\,{}^{N}H_yN_z$	${}^{N}H_x$	$-\,{}^{N}H_z$	${}^{N}H_z$	${}^{N}H_x$	$½\,(s^+_N + s^-_N)$
	N_x	N_x	$-2\,{}^{N}H_zN_y$	$-2\,{}^{N}H_xN_z$	$-{}^{N}H_y$	$-{}^{N}H_y$	$½\,(c^-_N - c^+_N)$

Table 1: Amide coherences at points a through f (Figure 1, S2). The negative sign of the ^{15}N gyromagnetic ratio was accounted for in all calculations. $c^+_N = \cos(\omega_N t_1 + \pi J_{NH} t_1)$, $c^-_N = \cos(\omega_N t_1 - \pi J_{NH} t_1)$, $s^+_N = \sin(\omega_N t_1 + \pi J_{NH} t_1)$, and $s^-_N = \sin(\omega_N t_1 - \pi J_{NH} t_1)$. $½\,(c^+_N + c^-_N) = \cos(\omega_N t_1)\cos(\pi J_{NH} t_1)$, etc. ω_N is the amide nitrogen frequency encoded during t_1 evolution, J_{NH} is the coupling constant between amide protons and nitrogens. ${}^{N}H$ refers to amide proton coherences.

	b	c	d	e	f	
A_1	$2\ ^{C}H_xC_z$	$-\ ^{C}Hy$	$-\ ^{C}Hz$	^{C}Hz	^{C}Hy	$\cos(\omega_C t_1)$
	$2\ ^{C}H_xC_x$	-	-	-	-	$\sin(\omega_C t_1)$
A_2	$-2\ ^{C}H_yC_x$	-	-	-	-	$\cos(\omega_C t_1)$
	$-2\ ^{C}H_yC_z$	^{C}Hx	$-\ ^{C}Hz$	^{C}Hz	$-\ ^{C}Hx$	$\sin(\omega_C t_1)$
A_3	$2\ ^{C}H_xC_z$	$-\ ^{C}Hy$	$-\ ^{C}Hz$	^{C}Hz	$-\ ^{C}Hy$	$\cos(\omega_C t_1)$
	$2\ ^{C}H_xC_x$	-	-	-	-	$\sin(\omega_C t_1)$
A_4	$-2\ ^{C}H_yC_x$	-	-	-	-	$\cos(\omega_C t_1)$
	$-2\ ^{C}H_yC_z$	^{C}Hx	$-\ ^{C}Hz$	^{C}Hz	^{C}Hx	$\sin(\omega_C t_1)$

Table 2: Methyl coherences at points b through f (Figure 1, S2). Quadrature detection for methyl carbons follows a States-TPPI[9] scheme. ω_C is the methyl carbon frequency encoded during t_1 evolution. ^{C}H refers to methyl protons.

	g
$A1_x$	$\frac{1}{2}\ ^{N}Hy\ (\ c^{+}_{N}\,c^{-}_{HN} - s^{+}_{N}\,s^{-}_{HN}\ + c^{-}_{N}\,c^{+}_{HN} + s^{-}_{N}\,s^{+}_{HN}) - {}^{C}H_y \cos(\omega_C t_1) \cos(\omega_{HC} t_2)$
$A2_x$	$\frac{1}{2}\ ^{N}Hy\ (-\ c^{+}_{N}\,c^{-}_{HN} + s^{+}_{N}\,s^{-}_{HN} + c^{-}_{N}\,c^{+}_{HN} + s^{-}_{N}\,s^{+}_{HN}) + {}^{C}H_y \sin(\omega_C t_1) \sin(\omega_{HC} t_2)$
$A3_x$	$\frac{1}{2}\ ^{N}Hy\ (-\ c^{+}_{N}\,c^{-}_{HN} - s^{+}_{N}\,s^{-}_{HN} - c^{-}_{N}\,c^{+}_{HN} + s^{-}_{N}\,s^{+}_{HN}) + {}^{C}H_y \cos(\omega_C t_1) \cos(\omega_{HC} t_2)$
$A4_x$	$\frac{1}{2}\ ^{N}Hy\ (-\ c^{+}_{N}\,c^{-}_{HN} - s^{+}_{N}\,s^{-}_{HN} + c^{-}_{N}\,c^{+}_{HN} - s^{-}_{N}\,s^{+}_{HN}) - {}^{C}H_y \sin(\omega_C t_1) \sin(\omega_{HC} t_2)$
$A1_y$	$\frac{1}{2}\ ^{N}Hy\ (\ c^{+}_{N}\,s^{-}_{HN} + s^{+}_{N}\,c^{-}_{HN} + c^{-}_{N}\,s^{+}_{HN} - s^{-}_{N}\,c^{+}_{HN}) - {}^{C}H_y \cos(\omega_C t_1) \sin(\omega_{HC} t_2)$
$A2_y$	$\frac{1}{2}\ ^{N}Hy\ (-\ c^{+}_{N}\,s^{-}_{HN} - s^{+}_{N}\,c^{-}_{HN} + c^{-}_{N}\,s^{+}_{HN} - s^{-}_{N}\,c^{+}_{HN}) - {}^{C}H_y \sin(\omega_C t_1) \cos(\omega_{HC} t_2)$
$A3_y$	$\frac{1}{2}\ ^{N}Hy\ (-\ c^{+}_{N}\,s^{-}_{HN} + s^{+}_{N}\,c^{-}_{HN} - c^{-}_{N}\,s^{+}_{HN} - s^{-}_{N}\,c^{+}_{HN}) + {}^{C}H_y \cos(\omega_C t_1) \sin(\omega_{HC} t_2)$
$A4_y$	$\frac{1}{2}\ ^{N}Hy\ (-\ c^{+}_{N}\,s^{-}_{HN} + s^{+}_{N}\,c^{-}_{HN} + c^{-}_{N}\,s^{+}_{HN} + s^{-}_{N}\,c^{+}_{HN}) + {}^{C}H_y \sin(\omega_C t_1) \cos(\omega_{HC} t_2)$

Table 3: Amide and methyl coherences after the mixing time at point g and evolution during t_2. A1 to A4 are recorded with ϕ_5= x ($A1_x$ to $A4_x$) and ϕ_5=y ($A1_y$ to $A4_y$), where the subscript denotes the phase of ϕ_5. $c^{+}_{HN} = \cos(\omega_{HN} + \pi J_{NH})t_2$, $c^{-}_{HN} = \cos(\omega_{HN} - \pi J_{NH})t_2$, $s^{+}_{HN} = \sin(\omega_{HN} + \pi J_{NH})t_2$, $s^{-}_{HN} = \sin(\omega_{HN} - \pi J_{NH})t_2$. ω_{HN} and ω_{HC} are the amide proton and methyl proton frequencies encoded during t_2 evolution.

Separation of ^{15}N and ^{13}C dispersed NOESY spectra.

To delineate the HN-TROSY-NOESY and HC-HSQC-NOESY spectra, $A1_x$ to $A4_x$ and $A1_y$ to $A4_y$ are all recorded with phase ω_2 =x and with ω_2 = -x in an interleaved manner, resulting in 16 separate acquisitions. Changing the phase of this pulse only changes the phase of detected methyl protons but leaves that of amide protons unaffected. The HN-TROSY-NOESY is obtained by adding both sets of signals and the HC-HSQC-NOESY by subtracting both sets of signals. Thus, after separation of pathways, 16 independent acquisitions have been condensed to 8 transients each for HN-TROSY-NOESY ($A1_{xN}$ – $A4_{xN}$ and $A1_{yN}$ – $A4_{yN}$) and HC-HSQC-NOESY ($A1_{xC}$ – $A4_{xC}$ and $A1_{yC}$ – $A4_{yC}$). These 8 transients are used for quadrature detection and line selection, as detailed below.

Quadrature detection for indirect dimensions, sensitivity enhancement and line selection.

Quadrature detection and line selection for HN-TROSY-NOESY is obtained by recombining $A1_x$ to $A4_x$ and $A1_y$ to $A4_y$ after separation of the ^{15}N and ^{13}C pathways. Quadrature detection for amide nitrogen and proton evolution periods, t_1 and t_2 respectively, is performed with a so-called Echo-AntiEcho sensitivity enhanced scheme. Real and imaginary components of the interferogram are obtained simultaneously as can be seen in Table 3. During processing, combination of the transients separates the real and imaginary components while simultaneously selecting for the slowly relaxing component of the HN multiplet (Table 4).

Quadrature Components	Transient Combinations	Signal
R (t_1) R (t_2)	$A1_{xN} + A2_{xN} - A3_{xN} + A4_{xN}$	$S_N e^{(-i \omega_H t_3)} c^-_N c^+_{HN}$
I (t_1) R (t_2)	$-(A1_{yN} + A2_{yN} + A3_{yN} - A4_{yN})$	$S_N e^{(-i \omega_H t_3)} s^-_N c^+_{HN}$
R (t_1) I (t_2)	$A1_{yN} + A2_{yN} - A3_{yN} + A4_{yN}$	$S_N e^{(-i \omega_H t_3)} c^-_N s^+_{HN}$
I (t_1) I (t_2)	$A1_{xN} + A2_{xN} + A3_{xN} - A4_{xN}$	$S_N e^{(-i \omega_H t_3)} s^-_N s^+_{HN}$

Table 4: Combination of transients for ^{15}N TROSY NOESY spectra. S_N is the amplitude of the signal before detection and ω_H is the frequency of the NOESY cross-peak encoded in the detected proton dimension (t_3). R & I refer to real and imaginary data for the respective evolution periods. The transients are now referred to as $A1_{xN}$ – $A4_{xN}$ and $A1_{yN}$ – $A4_{yN}$ to reflect that the amide and methyl pathways have been separated.

Sensitivity enhancement in the ^{15}N edited NOESY spectrum can only be achieved by storing transients separately. All eight transients (after ^{15}N and ^{13}C pathway separation) can then be used twice when performing quadrature detection; $A1_{xN}$, $A2_{xN}$, $A3_{xN}$ and $A4_{xN}$ are used to pro-

vide both $R(t_1)R(t_2)$ and $I(t_1)I(t_2)$ (and likewise $I(t_1)R(t_2)$ and $R(t_1)I(t_2)$ are obtained with $A1_{yN} – A4_{yN}$). In a conventional NMR acquisition, the receiver is used to perform such combinations. However, the receiver would select either the combination providing $R(t_1)R(t_2)$ or that providing $I(t_1)I(t_2)$ (the same is true for $R(t_1)I(t_2)$ and $I(t_1)R(t_2)$). Quadrature detection and TROSY line selection can still be achieved but a total of 16 transients need to be acquired, although half of the data are redundant. This doubling in experimental time results in a $\sqrt{2}$ loss in sensitivity when compared to separate storage of transients. The same method has been used before to perform sensitivity enhanced Echo-AntiEcho quadrature detection with ST2PT-TROSY schemes. [10,11]

In a conventional ^{13}C edited NOESY, hypercomplex data (RR, IR, RI, II) can be obtained by varying the phases ω_1 or ω_2 for methyl carbons and ϕ_3 or ϕ_5 for methyl protons. However, such a conventional implementation was not possible for methyl protons in our experiment. Indeed, the phases of ϕ_3 and ϕ_5 have been set to provide sensitivity-enhanced quadrature detection and HN-TROSY line selection for the amide pathway as discussed previously. Hence, the real and imaginary components of the methyl proton dimension are acquired in a nested manner (Table 3) as dictated by the phases imposed by the amide protons. The appropriate pairing of the transients i.e. $A1_{xC}$ to $A4_{xC}$ and $A1_{yC}$ to $A4_{yC}$ (Table 5) from such a nested acquisition provides hypercomplex data in the ^{13}C edited NOESY.

Quadrature Components	Transient Combinations	Signal
R (t_1) R (t_2)	$A1_{xC}$ - $A3_{xC}$	$S_c\, e^{(-i\,\omega_H\, t_3)} \cos(\omega_C t_1) \cos(\omega_{HC} t_2)$
I (t_1) R (t_2)	$A2_{yC} – A4_{yC}$	$S_c\, e^{(-i\,\omega_H\, t_3)} \sin(\omega_C t_1) \cos(\omega_{HC} t_2)$
R (t_1) I (t_2)	$A1_{yC}$ - $A3_{yC}$	$S_c\, e^{(-i\,\omega_H\, t_3)} \cos(\omega_C t_1) \sin(\omega_{HC} t_2)$
I (t_1) I (t_2)	-($A2_{xC}$ - $A4_{xC}$)	$S_c\, e^{(-i\,\omega_H\, t_3)} \sin(\omega_C t_1) \sin(\omega_{HC} t_2)$

Table 5: Combination of transients for ^{13}C HSQC NOESY spectra. Real and imaginary components are collected as dictated by the phase settings imposed by the HN-TROSY block and combined as shown. S_C is the amplitude of the signal before detection and ω_H is the frequency of the NOESY cross-peak encoded in the detected dimension (t_3). R & I refer to real and imaginary data for the respective evolution periods. The transients are now referred to as $A1_{xC} – A4_{xC}$ and $A1_{yC} – A4_{yC}$ to reflect that the amide and methyl pathways have been separated.

The separate storage of transients was also exploited to suppress artifacts in the ^{13}C -edited NOESY in a manner akin to phase cycling. The nested acquisition imposes that each component of the methyl proton dimension (R & I) be recorded twice. Since $A1_{xC}$ to $A4_{xC}$ and $A1_{yC}$ to $A4_{yC}$ can all be accessed during processing, various combinations can be used to retrieve real and imaginary components. Thus, the combinations shown in Table 4 can also produce RR, IR, RI, II. However such a combination results in artifacts in the ^{13}C edited NOESY spectrum. If instead the combinations of Table 5 are employed artifacts are suppressed. We exploited this advantage by reducing the size of phase cycling in our experiment.

In the end, 16 transients stored separately are efficiently used to i) separate ^{15}N and ^{13}C spectra ii) achieve sensitivity-enhanced quadrature detection in amide proton and nitrogen dimensions, iii) perform TROSY line selection, iv) obtain quadrature detection in methyl proton and carbon dimensions, and iv) suppress artifacts in ^{13}C edited NOESY. A single python script (available upon request) separates ^{15}N and ^{13}C dispersed spectra, combines the transients according to tables 4 and 5, and rearranges the data so that traditional NMRPipe[12] scripts can be used for processing (using the complex flag).

TS- NOESY- HN-TROSY/HC-HSQC (TS-NO-TR/HS)

The TS- NOESY- HN-TROSY/HC-HSQC (TS-NO-TR/HS) pulse sequence used to collect data in Figure 1 (main text) is an updated version of the previously published TS- NOESY- HN-TROSY/HC-SE-HSQC[13]. The pulse sequence is best described as an implementation of the pulse sequence of Permi and coworkers[2] to record NOESY spectra. In short, a NOESY block was added before the time-shared HN-TROSY/HC-HSQC published by Permi and coworkers[2] (Figure 1b, in J Biomol NMR (2007) 39:97–105). That is, the following pulse sequence was added:

$$\frac{\pi}{2}(^1H)^{\varphi5} - \delta2 - \pi(^1H)^{\varphi6} - \frac{t_2}{2} - \pi\left(\frac{^{15}N}{^{13}C}\right)^{x} - \frac{t_2}{2} - \frac{\pi}{2}(^1H)^{x} - \frac{\pi}{2}(^1H_2O)^{-x} - Gz - \delta g - t_m - \frac{\pi}{2}(^1H)^{\varphi7}$$

in which $\frac{\pi}{2}(^1H)^{\varphi5}$ denotes a 90° pulse of phase φ5 applied to protons. φ7 is the 1st 90° ^1H pulse in the pulse sequence of Permi and coworkers. The pulse phases for the NOESY block are: φ5 = x x -x –x, φ6 = y y -y -y, φ7= x x x x -x -x -x -x. The receiver phase cycling was modified to φ_{rec}=x -x x -x x -x x -x. The remaining pulses (other than φ7) follow those described in Permi's experiment. Quadrature detection in t_2 is performed with States-TPPI applied to φ5. The delay δ2 = 2*pw_N alleviates the need for first order phase corrections (pw_N is the length of the nitrogen 90° pulse). Gz is a pulsed-field gradient (33.5 G/cm) and δg is its associated recovery delay (200 μs). $\frac{\pi}{2}(^1H_2O)^{-x}$ is a water flip-back pulse preceding the first 90° pulse on proton in the pulse sequence of Permi and coworkers[2]. t_2 is the evolution period for ^1H encoding. tm is the mixing time (150 ms) corrected to account for the length of the pulsed field gradient, its recovery delay, and the water flip-back pulse. A few other minor modifications were made to the time-shared block[2] as follows. The SEDUCE-1 decoupling on the carbonyl carbons was not required because the protein sample used for data collection has a uniform ^{12}C labeled backbone. A single gradient pulse (1.65 ms, 40 G/cm) was used instead of bipolar gradients for ^{15}N encoding during the t_1 evolution period, to ensure satisfying water suppression. The two decoding gradients for amide protons (850 μs each, 4 G/cm) were implemented as described by Permi. REBURP shaped pulses (1.436 ms) were used for the methyl selective refocusing pulses as recommended[2].

Acquisition and Processing.

Both TS-TR/HS-NO and TS-NO-TR/HS spectra were acquired with 512 (^{1}H detected) x 150 (^{1}H indirect) x 30 (^{15}N/^{13}C indirect) complex points. The spectral widths in the detected ^{1}H and indirect ^{15}N/^{13}C dimensions were 16 ppm and 35 ppm / 24 ppm, respectively. The indirect ^{1}H dimension had a spectral width of 13 ppm for the TS-NO-TR/HS and 6.5 ppm for the TS-TR/HS-NO. The TS-NO-TR/HS was acquired with 16 scans per fid resulting in 64 transients when accounting for quadrature detection while the 16 transients of the TS-TR/HS-NO were acquired with 4 scans per transient since recombination of separately stored transients results in signal accumulation of 16 fids. A recycle delay of 1 s was used for both experiments. The acquisition times were 4 days, 7 hrs, 2 minutes for TS-TR/HS-NO and 4 days, 7 hrs, 16 minutes for TS-NO-TR/HS.

Both datasets were processed with the same cosine-squared bell apodization functions for the respective dimensions. Linear prediction was used to double the number of points in the indirect dimensions, which were subsequently zero-filled to 256 and 512 points in the^{15}N/^{13}C and ^{1}H dimensions, respectively. The detected dimensions were zero-filled to 1024 points before being Fourier transformed. NMRPipe[12] scripts were used to perform all the spectral processing mentioned above. All strips and overlays displayed in Figures 1 and 2 (main text) were created in CARA[14].

Non-Uniformly sampled TS-HN-TROSY/HC-HSQC-NOESY.

The non-uniformly sampled TS-HN-TROSY/HC-HSQC-NOESY spectra in Figure 2 of the main text was collected in the same time frame (4 days, 4 hrs, 48 min) and had the same spectral widths and acquisition parameters as its uniformly sampled counterpart. A sampling schedule spanning 45000 complex points (150 ^{15}N/^{13}C x 300 ^{1}H complex points) with a 10% sampling factor was generated with the software PoissonGap.[15]The seed used to generate the schedule was 12321. The HN-TROSY-NOESY and HC-HSQC-NOESY datasets were separated using the python script mentioned earlier and the indirect dimensions were reconstructed using the iterative soft thresholding software hmsIST[15] using 500 iterations per plane. Linear prediction was not used for the indirect dimensions. Apodization and zero-filling in the direct and indirect dimensions were performed as in the uniformly acquired dataset.

Considerations on the sensitivity of TS-TR/HS-NO and TS-NO-TR/HS experiments.

Many factors influence the sensitivity of each time-shared experiment. For idealized experiments, i.e. neglecting pulse lengths etc., the TS-TR/HS-NO benefits from up to 20 % in additional sensitivity because ^{15}N native magnetization can be exploited[11,16]. However, the TS-NO-TR/HS benefits further from the TROSY effect as protons evolving in the detected dimensions are involved. That is, a maximum of data points benefit from the TROSY effect. To these obser-

vations, one must add differences in spin manipulations that are inherent to each experiment. Thus, the TS-TR/HS-NO experiment requires a WATERGATE element while the TS-NO-TR/HS necessitates shaped pulses and refocusing periods.[2] For a rough estimation of the contribution of these factors to sensitivity, 1D traces of each experiment were compared with the software TOPSPIN 3.2.5. A mixing time of 10 ms was used to prevent nOe transfers but to allow for efficient water suppression. The TS-TR/HS-NO is more sensitive than TS-NO-TR/HS by 15% for amide moieties and 20% for methyl groups under the conditions used for acquiring the 3D experiments used in the manuscript. The 20 % difference in sensitivity for methyl groups mainly reflect the effects of spin manipulations in each experiment since methyl groups are subject to similar relaxation rates in both experiments. Our comparison highlights that spin manipulations necessary for gradient selection come at a high cost in signal to noise. This observation was a driving force in designing a TS experiment that relies on phase cycling instead of gradient selection.

In the context of 3D data acquisition, the TS-TR/HS-NO has an additional advantage over the TS-NO-TR/HS with regards to sensitivity. The TS-TR/HS-NO requires only half the spectral width in the indirect ^{1}H dimension and hence for the same resolution the number of scans can be doubled (i.e. $\sqrt{2}$ gain in sensitivity). In this study we have exploited this time saving to increase the resolution of the uniform TS-TR/HS-NO spectra and double the sampling factor for the NUS TS-TR/HS-NO spectra.

Peak Picking as a reporter of resolution.

In addition to the considerations described above, other factors contributed to decreasing the signal-to-noise in the 3D NOESY spectra acquired with the TS-NO-TR/HS. We observed a 20% sample precipitation between the acquisition of TS-TR/HS-NO and that of TS-NO-TR/HS, as monitored by 2D-HN-TROSY experiments. In addition, the apodization applied to the indirect proton dimension penalizes the TS-NO-TR/HS over the TS-TR/HS-NO since the former has a shorter maximum evolution time. That is, a higher number of intense data points are affected by the apodization in TS-NO-TR/HS than in TS-TR/HS-NO. For these reasons, fully automated peak picking would reflect a combination of sensitivity and resolution considerations. In order to focus solely on resolution differences between the spectra, the threshold for peak picking in the TS-TR/HS-NO was set to 1.5 times the threshold value of TS-NO-TR/HS. In contrast, the threshold for peak picking in the NUS dataset was set to the same level as that used in the uniform TS-TR/HS-NO dataset. Finally, peaks and signals were visually compared in each plane of the 3D datasets, at the threshold used during peak picking, to verify that no peak picked in the TS-TR/HS-NO reflected a signal that was absent at the threshold used in TS-NO-TR/HS. For these reasons, the numbers we provide in the main text reflect a lower estimate. Peak Picking in each spectra was performed using the program NMRDraw[12].

Cloning, expression and purification of Cy1.

All experimental data were recorded on a 52 kDa cyclization domain (Cy1) from the HMWP2 subunit of the *Yersinia pestis* yersiniabactin synthetase[17]. The ~1.4 kb fragment encompassing the Cy1 domain (residues 101 - 544) was amplified from pHMWP2.CH8[17] (a gift from Christopher Walsh's lab, Harvard Medical School) ligated into the pET30a expression vector (Novagen, San Diego, CA) and transformed into *E. coli* BL21(DE3) cells (Novagen). This construct expresses the Cy1 protein with LEHHHHHH appended to the C-terminus (construct named Cy1H6).

The NMR sample used in our studies is uniformly labeled with ^{2}H, ^{15}N, and ^{12}C, with ^{13}C ^{1}H labeling of the methyl groups of Ile (δ position only), Leu and Val side-chains, and with ^{15}N and ^{1}H labeling for Phe and Tyr residues. BL21(DE3) cells with the pET30a-Cy1H6 plasmid were initially grown in an overnight 50 mL LB medium at 37 °C (250 rpm). 1 mL overnight culture was used to inoculate 1 L of M9 minimal medium (6 g/L Na_2HPO4, 3 g/L KH_2PO_4, 0.5 g/L NaCl, 2 mM $MgCl_2$, 0.1 mM $CaCl_2$) in 99.9 % D_2O (Sigma/Aldrich) containing 2 g/L ^{2}H glucose (Cambridge Isotope Laboratories, CIL), 1g/L $^{15}NH_4Cl$ (Sigma/Aldrich), 10 mL vitamin solution (0.5 g/L thiamine, 0.1 g/L D-biotin, 0.1 g/L choline chloride, 0.1 g/L folic acid, 0.1 g/L Niacinamide, 0.1 g/L D-pantothenic acid, 0.1 g/L pyridoxal and 0.01 g/L riboflavin,in 99.9% D_2O), 2mL of trace element solution[18] (in 99.9% D_2O), and 50 mg/L kanamycin. At $O.D._{600}$ ~ 0.5, 75 mg of ^{13}C-methyl-α-ketobutyrate (CIL), 125 mg of $^{13}C_2$-dimethyl-α-ketoisovalerate (CIL), 150 mg ^{15}N-Tyrosine (CIL), 150 mg ^{15}N-Phenylalanine (CIL), were added. Once OD_{600} ~ 0.6, cells were chilled to ~16°C (ice bath), then protein expression was induced with 0.5 mM IPTG for an additional 12 hours 16°C x 250 rpm ($O.D._{600}$ ~ 1.4). Cell pellets were harvested by centrifugation (4°C, 5000 x g, 20 minutes) and were kept at -80°C until further use. Cell pellets were thawed on ice and resuspended in 50 mL of chilled Lysis buffer (50 mM Tris pH 8 at 4°C, 0.1 M NaCl, 5 mM Imidazole, 5 mM β-mercaptoethanol, 100 μg/mL Lysozyme, 50 μg/mL DNase I). All buffers used in the purification protocol were filtered with a 0.22 μm filter and degassed for 20 minutes before use. Cells were lysed with a microfluidizer (Microfluidics Inc. Waltham, MA) and cellular debris pelleted by centrifugation(4°C, 15000 x g, 30 minutes) followed by filtration using a 0.22 μm filter. The filtered lysate was loaded onto a 5 mL HisTrap HP column (GE Healthcare, Sweden) pre-equilibrated with His-Buffer A (50 mM Tris pH 8 at 4°C, 0.5 M NaCl, 5 mM Imidazole, 5 mM β-mercaptoethanol). The HisTrap column was washed with 100 mL of His-Buffer A at 4mL/min after loading the lysate and Cy1H6 was then eluted by a 0-100 % gradient of His-Buffer B (50 mM Tris pH 8 at 4°C, 0.5 M NaCl, 0.5 M Imidazole, 5 mM β-mercaptoethanol) at a flow rate of 3 mL/min. Cy1H6 containing fractions (confirmed by SDS-PAGE) were pooled and dialyzed overnight at 4°C against the Dialysis buffer (50 mM Tris pH 8 at 4°C, 0.1 M NaCl, 20 mM β-mercaptoethanol, 1mM EDTA). The dialysate was filtered (0.22 μm filter) and concentrated at 4°C using an Amicon Ultra centrifugal filter (10,000 NMWL, Millipore, Ireland) at 4000 x g to ~ 3 mL. The concentrated solution was injected in 1 mL batches onto a size exclusion chromatography (SEC) column (16/60 Superdex 200 pg column, GE Healthcare) equilibrated with SEC buffer (20 mM Sodium Phosphate buffer, 100 mM NaCl, 1 mM EDTA, 5 mM DTT, pH 7) at 0.7 ml/min. The single monodispersed peak containg Cy1H6 (ε_{280} = 88,265 M^{-1} cm^{-1}) was then concentrated and buffer exchanged into the NMR buffer (20 mM Sodium Phosphate, 10 mM NaCl, 1 mM EDTA, 5 mM DTT, pH 7.0) using 10,000 NMWL Amicon Ultra centrifugal filters (4°C, 2000 x g). The final NMR sample contained 5 % D_2O. All NMR experiments were conducted at 25 °C and the final protein concentration was 350 μM.

References:

(1) Piotto, M.; Saudek, V.; Sklenár, V. *J. Biomol. NMR* **1992**, *2*, 661–665.
(2) Würtz, P.; Aitio, O.; Hellman, M.; Permi, P. *J. Biomol. NMR* **2007**, *39*, 97–105.
(3) Shaka, A. J.; Reeler, J.; Frenkiel, T. O. M.; Freeman, R. A. Y. *J. Magn. Reson.* **1983**, *52*, 335–338.
(4) Van Ingen, H.; Vuister, G. W.; Tessari, M. *J. Magn. Reson.* **2002**, *156*, 258–261.
(5) Roehrl, M. H. A.; Heffron, G. J.; Wagner, G. *J. Magn. Reson.* **2005**, *174*, 325–330.
(6) Marion, D.; Wuthrich, K. *Biochem. Biophys. Res. Commun.* **1983**, *113*, 967–974.
(7) Farmer II, B. T. *J. Magn. Reson.* **1991**, *93*, 635–641.
(8) Boelens, R.; Burgering, M.; Fogh, R. H.; Kaptein, R. *J. Biomol. NMR* **1994**, *4*, 201–213.
(9) D. Marion, M. Ikura , R. Tschudin, A. B. *J. Magn. Reson.* **1989**, *85*, 393–399.
(10) Zhu, G.; Xia, Y.; Sze, K. H.; Yan, X. *J. Biomol. NMR* **1999**, *14*, 377–381.
(11) Brutscher, B.; Pardi, A.; Marion, D. *J. Am. Chem. Soc.* **1998**, *120*, 11845–11851.
(12) Delaglio, F.; Grzesiek, S.; Vuister, G. W.; Zhu, G.; Pfeifer, J.; Bax, A. *J. Biomol. NMR* **1995**, *6*, 277–293.
(13) Frueh, D. P.; Vosburg, D. A.; Walsh, C. T.; Wagner, G. *J. Biomol. NMR* **2006**, *34*, 31–40.
(14) Keller, R. L. J. The Computer Aided Resonance Assignment Tutorial; Cantina Verlag: Goldau, 2004.
(15) Hyberts, S. G.; Milbradt, A. G.; Wagner, A. B.; Arthanari, H.; Wagner, G. *J. Biomol. NMR* **2012**, *52*, 315–327.
(16) Pervushin, K. V.; Wider, G.; Wüthrich, K. *J. Biomol. NMR* **1998**, *12*, 345–348.
(17) Keating, T. A.; Miller, D. A.; Walsh, C. T. *Biochemistry* **2000**, *39*, 4729–4739.
(18) Cai, M.; Huang, Y., Sakaguchi, K.; Clore, M.G.; Gronenborn, A.M.; Craigie, R. *J. Biomol. NMR* 1998, *11*, 97–102